ELSEVIER

Earth and Planetary Science Letters 154 (1998) 307–322

EPSL

Anisotropic behavior of GRIP ices and flow in Central Greenland

O. Castelnau [a,*,1], H. Shoji [b], A. Mangeney [c,2], H. Milsch, P. Duval [d], A. Miyamoto [e], K. Kawada [f], O. Watanabe [g]

[a] *LPMTM–CNRS, Université Paris-Nord, Institut Galilée, Av. J.B. Clément, F-93430 Villetaneuse, France*
[b] *Kitami Institute of Technology, 165 Koen-Cho, Kitami, Hokkaido 090, Japan*
[c] *IPG Paris, Tour 24, 4 Place Jussieu, F-75005 Paris, France*
[d] *LGGE–CNRS, Domaine Universitaire, BP96, F-38402 St. Martin d'Hères Cedex, France*
[e] *Institute of Low Temperature Science, Hokkaido University, Kita-19, Nishi-8, Kita-ku, Sapporo 060, Japan*
[f] *Faculty of Science, Toyama University, 3190 Gofuku, Toyama 930, Japan*
[g] *National Institute of Polar Research, 9-10 Kaga 1-chome, Itabashi-ku, Tokyo 173, Japan*

Received 28 April 1997; accepted 9 October 1997

Abstract

Mechanical tests have been performed on strongly textured ice samples coming from a wide range of depths (from 1328 down to 2868 m) of the GReenland Ice core Project (GRIP) for different sample orientations with respect to the prescribed stress. In this way, two directional viscosities, corresponding to the ''easy glide'' and to the ''hard glide'' orientations, were determined along the core. The viscoplastic anisotropy gradually increases down to a depth of $\sim$2600 m and slightly decreases below, revealing a clear correlation between rheology and texture. The experimental mechanical response compares well with that predicted by the ViscoPlastic Self-Consistent (VPSC) model. The VPSC model is also applied to ice samples that exhibit an axisymmetric texture to show in more detail the sensitivity of the rheology to specific texture parameters. This leads to a number of recommendations for future mechanical tests on anisotropic samples. A large-scale ice flow model is finally used to estimate the influence of ice anisotropy on the flow along the GRIP–GISP2 flow line. The particular mechanical behavior of deep GRIP ices in the stress regime corresponding to an ice divide leads to deformation rates that are highly sensitive to bedrock topography and texture pattern. This feature is likely to favour the formation of stratigraphic disturbances in deep ice layers, as observed in the last 300 m of both GRIP and GISP2 cores. © 1998 Elsevier Science B.V.

Keywords: anisotropy; plasticity; ice; homogenisation; plastic flow

1. Introduction

This paper deals with the influence of ice rheology on the flow of ice sheets. In particular, the effects of the anisotropic behavior of polar ices will be investigated by: (1) analysing results of several mechanical tests performed on deep ices of the GReenland Ice core Project (GRIP); (2) modelling the mechanical behavior of polar ice with a micro–macro approach; and (3) modelling the large-scale flow of ice in the vicinity of the GRIP drill site (present summit of the Greenland ice cap).

Polar ice, as found in large ice masses like Green-

* Corresponding author. Tel.: +81-33-1-49-40-34.68;Fax: +81-33-1-49-40-39-38; E-mail: oc@lpmtm.univ-paris13.fr

[1] At LGGE–CNRS as this work was done.

[2] At LGGE–CNRS as this work was done.

PII S0012-821X(97)00193-3

land and Antarctica, is a polycrystalline material, meaning that it consists of an arrangement of crystals (grains). The macroscopic (bulk) mechanical behavior of an ice sample is directly linked to the microscopic (local) behavior of individual grains. Thus, it directly depends on the orientation of the crystallographic axes of grains with respect to the prescribed macroscopic deformation. Ice crystals exhibit an extreme viscoplastic anisotropy (they deform essentially by shear in basal planes). This means that the magnitude and direction of the deformation rate is highly dependent on the orientation of the prescribed stress with respect to the crystallographic axes. This microscopic anisotropy induces a strong macroscopic anisotropy when the polycrystalline sample exhibits a preferred orientation of the *c* axes (called ''texture'' in materials science). This is for example the case for Vostok (Antarctica), Dye 3 and Law Dome (Greenland) deep ices [1–3] and also for GRIP deep ices as will be shown here. Textures develop by the rotation of crystallographic planes during the plastic deformation that the ice is subjected to, and also when polygonization and migration recrystallization mechanisms are active [4,5]. When polar ice does not exhibit a particular orientation of the crystallographic axes (randomly oriented texture), as is the case for example for ice from the surface of ice sheets, the sample behaves identically in all directions and is said to be macroscopically isotropic.

The present paper raises the question of how the observed anisotropy may affect the flow of ice in ice sheets. In particular, we will show that it can make the flow near an ice divide extremely sensitive to bedrock topography and texture pattern. This feature could explain (at least partially) why the stratigraphy of the last 300 m of both GRIP and GISP2 ice cores is disturbed [6], a question of importance when attempting to reconstruct past climate from the study of deep ice cores.

We will present here results of several mechanical tests performed on GRIP ice samples of different depths, therefore presenting different textures. These tests were carried out in two different laboratories (LGGE-Grenoble, France, and Kitami Institute of Technology, Japan) for different orientations of the samples, so that different steady-state (secondary creep) directional viscosities could be determined at each depth (tertiary creep behavior of GRIP ices was presented by Dahl-Jensen et al. [7]). The comparison of all tests will show the good correlation between texture pattern and mechanical response. To understand in a more general way how textures influence the behavior of samples, we apply the ViscoPlastic Self-Consistent (VPSC) model of Lebensohn and Tomé [8] to GRIP ices. This model, which has already been used by Castelnau et al. [9–11], calculates an approximate solution of the stress and strain rate fields within the whole polycrystal, and thus estimates the mechanical response of a polycrystal for any prescribed stress when only the texture of the material is known. Using the texture of our GRIP samples as input to the model, we will compare the modelled rheology of GRIP ices with that determined experimentally. This is to our knowledge the first time that a rheological model for anisotropic ices is tested quantitatively on mechanical tests performed in the laboratory. The VPSC model enables us also to investigate how the sample behavior is sensitive to specific texture parameters and in particular to texture symmetries, an important question as shown by Azuma and Goto-Azuma [12]. In the last part of this paper, we study how ice anisotropy may affect the large-scale flow of ice in Central Greenland. For this, we apply the large-scale ice flow model developed by Mangeney et al. [13,14] to the GRIP–GISP2 flow line. This model takes into account an anisotropic constitutive relation which gives the rheology of the ice for a given texture [15]. At present, the model is restricted to textures that exhibit an axisymmetry around the in situ vertical axis (i.e. the vertical axis is a revolution axis for the texture). This is due to the fact that all analytical anisotropic constitutive relations for polar ice have so far been developed for ices presenting orthotropic transversally isotropic behavior. In fact, such a texture symmetry is found only approximately in natural samples [16]. We will show that this approximation should lead to significant inaccuracy in flow prediction. Consequently, the flow of ice near an ice divide cannot be realistically modelled unless a model is developed that precisely describes the development of texture with deformation and recrystallization.

The present paper is structured as follows. In Section 2, we present the results of mechanical tests. In Section 3, we compare the results of the VPSC

model with those obtained experimentally, and we show in more detail how texture symmetries affect polycrystal behavior. In Section 4, we apply the large-scale ice flow model to Central Greenland to show how anisotropy influences the in situ flow.

2. Experiments

2.1. Description

Several mechanical tests have been performed on GRIP ice samples taken from depths ranging from 1328 to 2868 m. The texture of GRIP ices, described in detail by Thorsteinsson et al. [17], changes along the core from a random orientation at the ice sheet surface to a strongly preferred orientation in the deeper parts, with *c* axes aligned approximately parallel to the in situ vertical direction. This vertical single maximum texture becomes pronounced at 2200 m and persists down to a depth of 2800 m. No sharp contrast in the texture is observed across the Holocene–Wisconsin climatic transition (1625 m). From 2800 to 3028 m (bedrock), textures are less pronounced, due to the effects of migration recrystallization. The initial *c* axis textures of our samples are shown in Fig. 1. Here, the compressive axis ($z'z$) corresponds to the centre of the pole figures. Post-deformation thin sections were cut from each sample to check that there was no texture evolution during the mechanical tests. The increasing concentration of textures with depth can be observed qualitatively on the pole figures. To quantify this concentration, we define a statistical parameter referred to as the strength of orientation *R*. The *c* axis of each grain *g* being treated as a unit vector (denoted $\boldsymbol{c}^g$), the

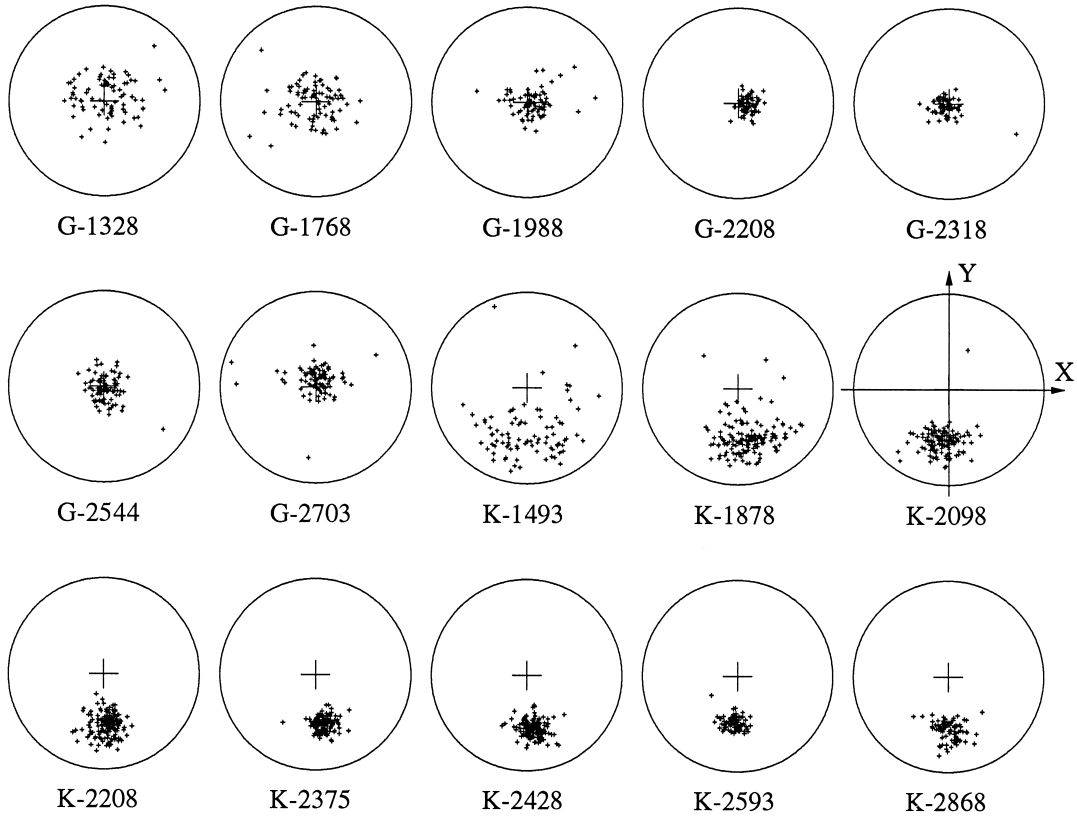

Fig. 1. *c* axis textures of GRIP samples tested in Grenoble (G-) and in Kitami (K-). Depths are given in meters. The centre of the pole figures ($z'z$ axis) indicates the direction of compression. It corresponds to the in situ vertical direction for samples tested in Grenoble (G-1328 to G-2703).

strength of orientation is proportional to the norm of the sum of all $\boldsymbol{c}^g$ vectors so that:

$$R\,\% = \left(\frac{2}{N} \left\| \sum_{g=1}^{N} c^g \right\| - 1 \right) \times 100 \qquad (1)$$

where N is the total number of grains in the thin section. The parameter R is equal to 0% for a randomly oriented texture and takes on a maximal value of 100% when all c axes are exactly parallel. The evolution of R with depth is shown in Fig. 2a. We clearly see an increase from 1000 down to 2600 m depth, and a decrease below.

Deformation conditions prescribed in Grenoble and Kitami were different. In Grenoble, test pieces were cut in the direction of the core axis (which was drilled vertically in the ice cap), and a uniaxial compressive stress was applied in that direction. In Kitami, uniaxial compression tests were performed on test pieces inclined at 45° from the core axis. Owing to deviation of a few degrees between (1) the core axis and the in situ vertical direction and (2) the sample axis and core axis, Grenoble experiments make it possible to determine the directional viscosity for compression along a nearly vertical in situ axis, and Kitami experiments for shear in a nearly horizontal in situ plane combined with uniaxial tension along a nearly horizontal in situ direction (see Appendix A). We will see later that this slight misorientation of sample axes with respect to the in situ axes cannot be neglected when estimating the rheology of the ice in the ice sheet. The size of all samples was similar, with a diameter of 30 mm and a length of 75 mm, approximately. A depth dependence of the mean grain size was observed at GRIP [17]. In our samples, the mean grain size ranges from 1.1 to 6.1 mm. Performing mechanical tests on strongly anisotropic samples requires paying special attention to the prescribed boundary conditions, as will be shown below. Here, the friction between sample surfaces and the apparatus platen was minimized, so that we can consider that the prescribed compressive stress was the only non-zero component of the stress tensor and that no component of the strain rate tensor was constrained. This was achieved in Grenoble by inserting thin Teflon sheets between the sample surfaces and the apparatus platen and in Kitami by applying Silicone oil at the beginning of each test run. Tests were performed under both

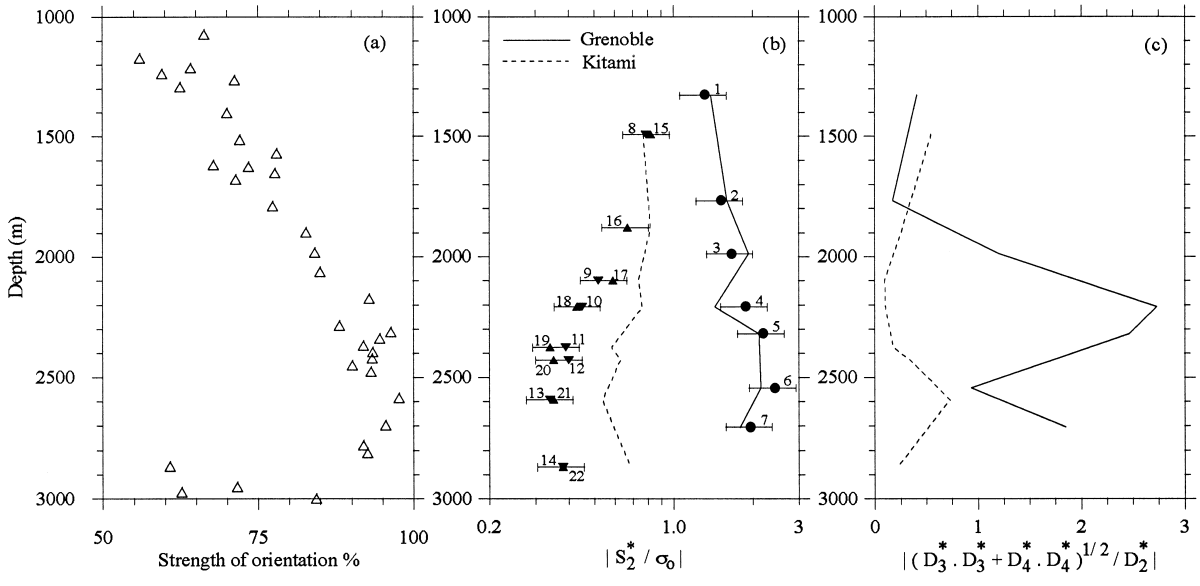

Fig. 2. (a) Evolution with depth of the strength of orientation.
(b) Experimental flow stress $|S_2^*/\sigma_0|$ for both Grenoble (tests 1–7) and Kitami (8–22) tests (*dots*), as compared to VPSC modelled rheology (*lines*).
(c) Shear response of samples to a uniaxial compression test, calculated with the VPSC model.

constant load (creep) and constant cross-head speed conditions.

Generally, steady-state ice behavior is described by the secondary creep. In Kitami tests, the deformation of samples was larger than 1% for all samples, so that the secondary creep stage was effectively reached. In the Grenoble tests, due to the much smaller deformation rate, experiments were stopped when the axial deformation reached $\sim 0.6\%$. The minimum creep rate was extrapolated using the Andrade law [18] which was found to match the primary creep well. This correction remains small since the extrapolated minimum strain rate was smaller than the measured minimum strain rate by only $\sim 20\%$. Experimental test conditions are summarized in Table 1, where tests are numbered from 1 to 22. Tests 1–7 are Grenoble tests, and tests 8–22 are Kitami tests. Axial strain rates and axial stresses corresponding to the minimum creep rate are indicated. Stationary axial strain rates are found to range from 3.0×10^{-10} to 8.24×10^{-8} s^{-1} for axial stresses ranging from 0.21 to 0.81 MPa. It should be noted that Grenoble samples are generally more stressed than Kitami samples, but they deform much slower by at least one order of magnitude. Qualitatively, this difference originates from the fact that in the Grenoble tests, the basal planes of grains are nearly orthogonal to the prescribed macroscopic stress, so that the resolved shear stress in basal planes (and therefore the strain rate of grains) is minimum. In the Kitami tests, the resolved shear stress in the basal planes is maximum, inducing a large strain rate for all grains, i.e. for the whole sample. This large difference between results of the two laboratories clearly highlights the very large viscoplastic anisotropy of deep GRIP samples.

Table 1
Test number, bag number, in situ depth, test temperature, axial (compressive) stress and strain rate corresponding to the secondary creep stage, and experimental relative flow stress S_2^*/σ_0 calculated at -10°C, for the Grenoble (1–7) and Kitami (8–22) tests

No.	Bag No.	Depth (m)	Temp. (°C)	$-\sigma_{ax}$ (MPa)	$-D_{ax}$ (10^{-9} s^{-1})	$-S_2^*/\sigma_0$ @ -10°C
1	2415	1328	−10	0.63	6.4	1.32
2	3215	1768	−10	0.64	3.7	1.53
3	3615	1988	−10	0.66	2.9	1.67
4	4015	2208	−10	0.62	1.4	1.90
5	4215	2318	−10	0.64	0.87	2.20
6	4625	2544	−10	0.51	0.30	2.43
7	4915	2703	−10	0.62	1.2	1.98
8	2714	1493	−15	0.68	31.7	0.79
9	3814	2098	−15	0.51	71.0	0.52
10	4014	2208	−15	0.35	39.5	0.45
11	4318	2375	−15	0.33	62.7	0.39
12	4414	2428	−15	0.36	69.0	0.40
13	4715	2593	−15	0.21	25.7	0.34
14	5214	2868	−15	0.36	82.4	0.38
15	2714	1493	−15	0.81	45.6	0.82
16	3415	1878	−15	0.61	45.1	0.67
17	3814	2098	−15	0.52	45.1	0.59
18	4014	2208	−15	0.34	45.8	0.43
19	4318	2375	−15	0.25	44.3	0.34
20	4414	2428	−15	0.26	45.3	0.35
21	4715	2593	−15	0.26	43.9	0.35
22	5214	2868	−15	0.28	40.3	0.38

Tests 1–14 are creep tests. Tests 15–22 are constant cross-head speed tests.

2.2. Comparison of results

We have presented the experimental mechanical response of several GRIP ice samples deformed under uniaxial compression for two different orientations of the texture with respect to the applied compressive stress. The tests were performed under different conditions, i.e. for different stresses and strain rates at the secondary creep stage and for slightly different temperatures. Now, results of all these tests will be compared. But to do this, it is necessary to find a common criterion for expressing experimental results, as presented below.

To describe general anisotropy, it is convenient to define a stress potential ϕ such that:

$$D_{ij} = \frac{\partial \phi}{\partial S_{ij}} \tag{2}$$

and to plot the equipotential surfaces in the stress space. Since only 5 components of the strain rate $\boldsymbol{D}$ and the Cauchy deviatoric stress $\boldsymbol{S}$ are independent (both are traceless symmetric tensors), it is more convenient to express $\boldsymbol{D}$ and $\boldsymbol{S}$ tensors in a 5-dimen-

sional space. Here, we use the transformation proposed by Lequeu et al. [19]:

$$\begin{cases} D_1 = (D_{22} - D_{11})/\sqrt{2} \\ D_2 = \sqrt{3/2}\, D_{33} \\ D_3 = \sqrt{2}\, D_{23} \\ D_4 = \sqrt{2}\, D_{13} \\ D_5 = \sqrt{2}\, D_{12} \end{cases} \quad (3)$$

(and identically for $\boldsymbol{S}$), and we call independently $\boldsymbol{D}$ and $\boldsymbol{S}$ the second-order tensors (with components D_{ij} and S_{ij}) or the 5-D vectors (with components D_i and S_i). The components D_1 and D_2 represent axial strain rates, whereas D_3, D_4 and D_5 are shear rates (and similarly for $\boldsymbol{S}$). This transformation conserves the contracted product:

$$S_{ij} D_{ij} = S_i D_i \quad (4)$$

(with summation over repeated indices). Usually, the potential ϕ is assumed to be proportional to the work rate $W = S_{ij} D_{ij}$. However, as explained by Castelnau et al. [11], such a simple relation is not found with the VPSC model. Consequently, ϕ cannot be determined easily. For this reason, we use a slightly different approach here. We express all experimental results for a given value of the work rate W. To do this, we multiply the stress vector by a dimensionless factor k^*:

$$k^* = \sqrt{\frac{3}{2}} \left(\frac{\dot{\gamma}_0 \sigma_0}{\dot{W}} \right)^{1/(n+1)} \quad (5)$$

and then strain rate vector by k^{*n} for sake of homogeneity. Here, σ_0 is a reference stress the meaning of which is explained below, and $\dot{\gamma}_0$ is a reference strain rate taken as equal to unity ($\dot{\gamma}_0 = 1\ s^{-1}$). We denote $\boldsymbol{S}^*$ and $\boldsymbol{D}^*$ the resulting deviatoric stress and strain rate vectors, respectively. The new work rate then has a constant value:

$$\dot{W}^* = S_i^* D_i^* = \left(\sqrt{\frac{3}{2}} \right)^{n+1} \dot{\gamma}_0 \sigma_0 \quad (6)$$

The reference stress σ_0 is linked to the isotropic viscosity. It appears in the Norton relation:

$$D_i = \frac{3}{2} \dot{\gamma}_0 \frac{S_{eq}^{n-1}}{\sigma_0^n} S_i \quad (7)$$

which we use to describe the behavior of isotropic polycrystalline ice, where S_{eq} is the Von Mises equivalent stress given by $S_{eq} = \sqrt{\frac{3}{2} S_i S_i}$. Note that Eq. (7) is completely equivalent to the so-called ''Glen flow law'' generally adopted in glaciology:

$$D_i = \frac{B_0}{2} \tau_e^{n-1} S_i \quad (8)$$

if the reference stress σ_0 is expressed as a function of the flow law coefficient B_0:

$$B_0 = \dot{\gamma}_0 \frac{\left(\sqrt{3}\right)^{n+1}}{\sigma_0^n} \quad (9)$$

The advantage of Eq. (7) as compared to Eq. (8) is that σ_0 has the dimension of a stress whereas B_0 has a mixed dimension. At this point, it can easily be shown that with the particular value of the work rate W^* we have chosen, all equipotential surfaces corresponding to the isotropic Norton behavior are represented in the new S_i^* axes by a unique hypersphere of radius σ_0. For anisotropic samples, small values of $|S_i^*|$, as compared to σ_0, indicate a soft response of the polycrystal (small directional viscosity), and large $|S_i^*|$ values a hard response (large directional viscosity). The $z'z$ axis being the compression axis in both the Grenoble and Kitami tests, only the S_2^* stress component has a non-zero value. Therefore, S_2^* value is directly linked to the so-called ''enhancement factor'' E_s by the relation:

$$E_s = \left(\frac{\sigma_0}{|S_2^*|} \right)^{n+1} \quad (10)$$

where E_s is a scalar often introduced in the isotropic Glen flow law:

$$D_i = E_s \frac{B_0}{2} \tau_e^{n-1} S_i \quad (11)$$

to describe the directional response of anisotropic samples [20].

We express all experimental relative flow stresses S_2^*/σ_0 for a temperature of $-10°C$ using an activation energy $Q = 78$ kJ/mol [21], see Table 1. The commonly adopted value of the stress exponent is $n = 3$ for equivalent stresses larger than 0.2 MPa [22]. According to Budd and Jacka's experimental results [3] and accounting for experimental uncertain-

ties, the σ_0 value is estimated to be equal to 234 MPa $\pm$ 25% at -10°C. Furthermore, we estimate the uncertainty in S_2^* to be $\pm$20%. This value takes into account: (1) the uncertainty in $\sigma_{0;}$ (2) that during a creep test, the strain rate is determined to within about a factor 1.5; and (3) during a constant cross-head speed test, the uncertainty in the stress is 10%.

Experimental S_2^*/σ_0 values are plotted vs. in situ depth in Fig. 2b. We clearly see the increasing anisotropy of GRIP ices, from the surface down to 2600 m depth, since the difference between Grenoble and Kitami $|S_2^*/\sigma_0|$ values gradually increases with depth. This feature is clearly linked to the increasing strength of texture, see Fig. 2a. Below 2600 m, GRIP ices become slightly less anisotropic, due to a slightly decreasing texture strength. We thus find a clear experimental correlation between texture concentration and mechanical response. At 2500 m depth, Grenoble and Kitami S_2^*/σ_0 values are $\sim$2.4 and $\sim$0.35, respectively, i.e. corresponding to enhancement factors of $\sim$0.03 and $\sim$65, respectively, as compared to the isotropic behavior given by Budd and Jacka [3]. Under Grenoble test conditions, the enhancement factors are comparable to those previously obtained on Law Dome [21] and Dye 3 [23] samples, which exhibit textures similar to those of GRIP ices. Under Kitami test conditions, however, they are larger than expected. For example, they are 2 to 3 times larger than those obtained on Dye 3 ices [24]. This discrepancy cannot originate from experimental error. Indeed, one creep test and one constant cross-head speed test were performed for each sample (except K-1878), and both tests lead to very similar results. However, precise observation of the Kitami samples after tests were performed shows slightly heterogeneous deformations within the samples which were prepared from cloudy band layers (a cloudy band is a layer with a high concentration of microscopic inclusions diffracting light; the nature of such bands is not well defined and their occurrence generally correlates with a high dust content [7]). Additional tests indicate: (1) some cloudy band ice is softer than adjacent clear ices above and below; and (2) boundary slide sometimes takes place between cloudy and clear ice zones. These findings are likely to explain why GRIP ices are so soft under the Kitami test conditions. A detailed study on the influence of cloudy bands will be published elsewhere.

3. Modelling mechanical behavior

Mechanical tests have been used to determine the response of GRIP ice samples for two different orientations of the stress state with respect to texture orientation. To understand in a more general way the relation between texture and rheology, we use a micro–macro model, i.e. a model that relates the behavior of the polycrystal to that of individual grains. We shall now concentrate on the comparison between the experimental rheology of our GRIP samples and that predicted by the model. Afterwards, we will use the VPSC model to study the influence of some specific texture parameters (namely texture concentration and texture symmetries) on the mechanical response.

3.1. Description of the VPSC model

We use the VPSC model formulated in an alternative framework by Molinari et al. [25] and applied it to anisotropic materials by Lebensohn and Tomé [8]. This model can be used to calculate texture development for large deformations. Here, it will be applied solely to calculate the *instantaneous* response (no texture development) of anisotropic polycrystals, i.e. the response corresponding to the experimental secondary creep stage.

Basically, the VPSC model gives a first-order solution to the set of stress equilibrium and incompressibility equations applied over the entire polycrystal volume. Each grain of the polycrystal is regarded as an ellipsoidal viscoplastic inclusion deforming in a viscoplastic Homogeneous Equivalent Medium (HEM) having the average properties of the polycrystal. This treatment leads to an interaction equation that linearly relates the deviations of the stress and strain rate in grains with respect to the (macroscopic) stress and strain rate of the HEM. The condition that the average of stress and strain rate over all grains has to be consistent with the equivalent macroscopic magnitudes, ensures a self-consistent solution to the problem. Consequently, stresses and strain rates are different in each grain. The deviation of local behavior with respect to macroscopic behavior depends on the directional viscoplastic properties of the grains and the whole polycrystal.

This model requires the use of a constitutive relation for the grains. Here, the shear rate $\dot{\gamma}^s$ which results from dislocation motion on a slip system s is a function of the resolved shear stress τ_r^s on that system:

$$\dot{\gamma}^s = \dot{\gamma}_0 \left| \frac{\tau_r^s}{\tau_0^s} \right|^{n-1} \frac{\tau_r^s}{\tau_0^s} \quad (12)$$

where τ_0^s is the Reference Resolved Shear Stress (RRSS) that expresses the hardness of the slip system s, in a similar way as with σ_0 for an isotropic polycrystal (Eq. (7)). The resolved stress τ_r^s is calculated from the local deviatoric stress $\boldsymbol{S}^g$:

$$\tau_r^s = r_{ij}^s S_{ij}^g \quad (13)$$

where $\boldsymbol{r}^s$ is a geometric tensor (the Schmid tensor) that depends solely on the orientation of the slip system s with respect to the reference frame. The strain rate in the grain g reads:

$$D_{ij}^g = \sum_s \dot{\gamma}^s r_{ij}^s \quad (14)$$

This last relation is rewritten in a pseudo-linear form:

$$D_{ij}^g = M_{ijkl}^g S_{kl}^g \quad (15)$$

with $\boldsymbol{M}^g$ denoting the compliance tensor of grain g. A similar form is taken for the constitutive relation of the polycrystal:

$$D_{ij} = M_{ijkl} S_{kl} \quad (16)$$

The macroscopic compliance $\boldsymbol{M}$, which depends on macroscopic stress and material structure, is not known in advance. The inclusion problem of a grain embedded in a HEM is solved by extending the classical results of Eshelby for linear elasticity [26] to non-linear viscoplasticity. This treatment leads to an interaction equation that relates microscopic and macroscopic magnitudes:

$$D_{ij}^g - D_{ij} = -\tilde{M}_{ijkl}\left(S_{kl}^g - S_{kl}\right) \quad (17)$$

The interaction tensor $\tilde{\boldsymbol{M}}$ can be expressed as a function of the grain shape, the macroscopic compliance $\boldsymbol{M}$, and the prescribed macroscopic stress. This treatment makes it possible to calculate the mechanical response (i.e. the tensor $\boldsymbol{M}$) of a sample, given its initial texture and the intracrystalline deformation mechanism of the material (i.e. $\boldsymbol{r}^s$ tensors of all grains and RRSS values). The principal limitations of the VPSC model are that: (1) deformation is assumed to be uniform within each grain; (2) interaction between directly neighboring grains is not taken into account; and (3) the macroscopic constitutive relation (16) must be linearized in the vicinity of the prescribed macroscopic stress. However, this model presents the advantage of providing a good estimation of polycrystal behavior at a relatively limited numerical cost.

3.2. Comparison with experiments

The modelled mechanical response of a textured polycrystal completely depends on the microscopic rheological parameters, that is on the RRSS of each slip system. Here, ice crystals are assumed to deform by dislocation glide on basal $\{0001\}\langle 11\bar{2}0\rangle$, prismatic $\{01\bar{1}0\}\langle 2\bar{1}\bar{1}0\rangle$, and pyramidal $\{11\bar{2}2\}\langle 11\bar{2}\bar{3}\rangle$ systems. The RRSS of basal systems is adjusted so that the model reproduces the viscosity of an isotropic polycrystal (i.e. the value of σ_0), and the prismatic and pyramidal RRSSs are assumed to be 70 times larger than basal RRSSs [27,11]. These values, which are in good agreement with the behavior of isolated single crystals given by Duval et al. [18], lead to the best reproduction of the experimental behavior of two strongly textured samples of the Vostok (Antarctica) ice core deformed under uniaxial and biaxial compression with different orientations of the texture with respect to the prescribed deformation.

We shall now apply the VPSC model to the Grenoble and Kitami experiments. Measured textures of samples (Fig. 1) were introduced in the model, and calculations were carried out for conditions corresponding to a frictionless contact between the sample surfaces and the apparatus platen, i.e. with $\boldsymbol{S} = (0,S_2,0,0,0)$. No boundary conditions were imposed on the strain rate $\boldsymbol{D}$, which was determined exclusively by numerical means. The relative axial deviatoric flow stress $|S_2^*/\sigma_0|$ calculated with the model is plotted in Fig. 2b as a function of in situ depth. Qualitatively, the VPSC model successfully reproduces experimental behaviors, with a gradually increasing anisotropy to a depth of 2600 m, and a slowly decreasing anisotropy below. Quantitatively, we find very good agreement for all Grenoble experiments, indicating that the model well reproduces the

relation between texture and rheology. Poorer quantitative agreement is obtained for the Kitami samples. The minimal modelled value of $|S_2^*/\sigma_0|$ is 0.54, i.e. corresponding to an enhancement factor of only 12, which indicates a higher directional viscosity than the one determined experimentally. To explain this discrepancy, the inaccuracies resulting from the assumptions of the VPSC formulation cannot be completely disregarded. However, we found that the VPSC model successfully reproduces the experimental viscosities of ice samples exhibiting different textures (Grenoble GRIP, Vostok, Law Dome) and deformed under very different stress conditions (uniaxial and biaxial compression, torsion, and torsion-compression) [27]. Therefore, we suggest that the differential deformation in cloudy band layer ice, as observed experimentally, which leads to a lower viscosity and which is not taken into account in the model, is likely to explain this discrepancy.

Fig. 2c presents the modelled deformation rates of GRIP samples under the present experimental conditions. It shows the total shear strain rate $(D_3^{*2} + D_4^{*2})^{1/2}$ in the plane orthogonal to the compression axis, relative to the axial strain rate D_2^*. The shear strain rate of the Grenoble samples reaches high values, with a maximum (~ 2.7) for G-2208. Such values indicate that the Grenoble samples mainly deform by shear in response to a compressive stress S_2^*. This necessarily induces a considerable displacement of sample surfaces on the compression apparatus platen which should attain here 3 mm (1/10th of the sample diameter!). It is important to note that this behavior is qualitatively model-independent, since it has been found with two other very different micro–macro models, namely the uniform stress and uniform strain rate models. An effort should be made in the future to measure this deformation experimentally. The shear strain rate component of the Kitami samples is much lower. This is a surprising result since the texture axis deviated significantly from the compressive axis. This point will be investigated below.

At this stage, it is apparent that texture pattern significantly affects the mechanical response of samples. Globally, a good agreement between experimental and modelled rheology was found. Furthermore, the VPSC model shows that a significant shear deformation appears while compressing Grenoble samples, a feature that is not easy to understand since natural texture patterns are complex. In the next section, we investigate the rheology of samples exhibiting ideal axisymmetric textures. This will enable us to show more precisely the sensitivity of mechanical behavior to texture orientation.

3.3. Rheology of samples with axisymmetric texture

The advantage of studying the rheology of samples for which the texture exhibits particular symmetries is that the form of the strain rate tensor can be qualitatively determined given the form of the prescribed stress. For example, as shown by Canova et al. [28], a stress of the form $\boldsymbol{S} = (S_1, S_2, 0, 0, 0)$ applied on a sample exhibiting a texture that is axisymmetric around the $z'z$ axis leads to a strain rate of the form $\boldsymbol{D} = (D_1, D_2, 0, 0, 0)$, and $\boldsymbol{S} = (0, 0, S_3, 0, 0)$ leads to $\boldsymbol{D} = (0, 0, D_3, 0, 0)$. Following Canova et al., we call the subspaces $\{S_1, S_2\}$ and $\{S_3\}$ ''closed''. Note that for polar ices (including GRIP), textures reflect the whole in situ deformation history (which is complex) of the ice sample and thus never exhibit strict symmetry. For GRIP ices, textures are approximately symmetric around the in situ vertical axis, but $\{S_1, S_2\}$ is not an approximately closed subspace at all, since the shear rate components D_3 and D_4 are far from negligible for $\boldsymbol{S} = (0, S_2, 0, 0, 0)$, as shown above.

We now consider a sample for which the texture is axisymmetric around an axis that lies in the yz plane, and we call δ_s the angle between the $z'z$ axis and this revolution axis. Thus, the yz plane is a plane of symmetry, which induces the closeness of the $\{S_1, S_2, S_3\}$ subspace [28]. The concentration of the texture is assumed to be similar to that of deep GRIP samples. Fig. 3a shows, for example, the texture corresponding to $\delta_s = 10°$. We shall now first look at the sensitivity of the mechanical response on the orientation of the texture with respect to the prescribed stress, and then we will study the response of two samples ($\delta_s = 0°$ and $\delta_s = 10°$) deformed under various stress conditions.

For various values of δ_s, we calculate the behavior of samples deformed under uniaxial compression in the $z'z$ direction, i.e. for $\boldsymbol{S}^* = (0, S_2^*, 0, 0, 0)$. The closeness of $\{S_1^*, S_2^*, S_3^*\}$ implies that $\boldsymbol{D}^*$ takes the form $\boldsymbol{D}^* = (D_1^*, D_2^*, D_3^*, 0, 0)$. To express the orien-

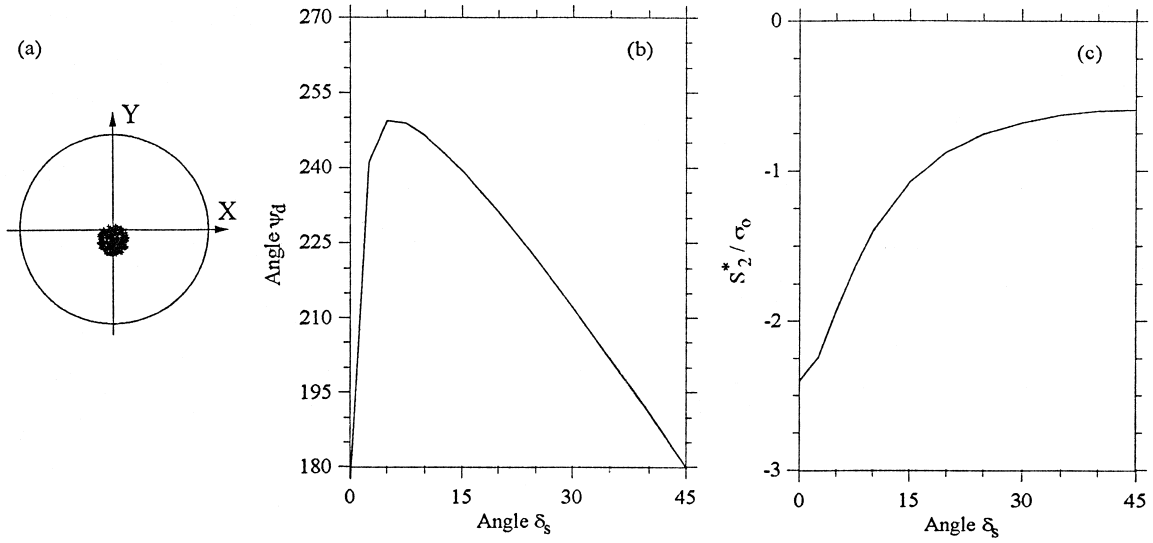

Fig. 3. Response calculated with the VPSC model of a polycrystal exhibiting an axisymmetric texture, as a function of the angle δ_s between the revolution axis of the texture and the direction $z'z$ of uniaxial compression.
(a) Texture corresponding to $\delta_s = 10°$.
(b) Direction of the strain rate vector in the $\{S_2^*, S_3^*\}$ subspace.
(c) Relative axial flow stress.

tation of $\boldsymbol{D}^*$, we define the angle ψ_d between the projection of the vector $\boldsymbol{D}^*$ on the $\{S_2^*, S_3^*\}$ plane and the S_2^* axis, as shown in Fig. 4. Results are plotted in Fig. 3. For Grenoble-like experiments ($\delta_s \approx 0°$), we observe significant influence of texture orientation on the orientation of the strain rate vector. The sample only deforms axially for $\delta_s = 0°$ (since $\psi_d = 180°$), but mainly deforms by shear for $\delta_s = 2.5°$ only (since $\psi_d = 240°$, i.e. $D_3^* \approx 1.7 D_2^*$). The flow stress is also very sensitive to δ_s. We obtain $|S_2^*/\sigma_0| = 2.40$ for $\delta_s = 0°$, and $|S_2^*/\sigma_0| = 1.40$ for $\delta_s = 10°$, i.e. a 10° rotation of the texture increases the enhancement factor by a factor of 8! For natural GRIP ices, textures do not exhibit any symmetry. Consequently, it is practically impossible to conduct Grenoble-like experiments on GRIP ices such that the shear deformation of samples is negligible. Note that this shear deformation leads to experimental difficulties, since it induces a non-uniform distribution of axial stress on sample surfaces. It is allowed only if special care is taken to avoid friction between the sample surfaces and the apparatus platen. Different behavior is found for Kitami-like experiments ($\delta_s \approx 45°$). For idealized test conditions, i.e. $\delta_s = 45°$, the sample only deforms axially. In fact, as shown in Appendix A, this feature is not necessarily observed for weakly textured samples. No significant shear deformation appears for slight variations of δ_s around the 45° ideal value, and the flow stress is found to be only slightly sensitive to δ_s. Consequently, Kitami experiments on natural GRIP ices provide a good measurement of the directional viscosity corresponding to an in situ horizontal shear combined with a horizontal uniaxial tension.

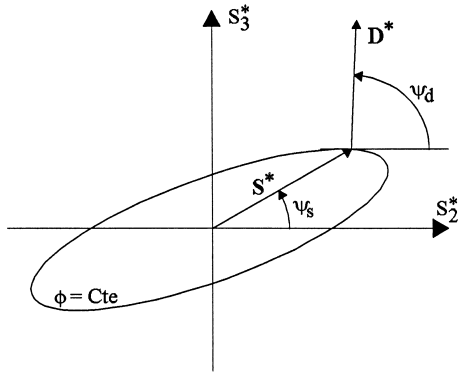

Fig. 4. The angles ψ_s and ψ_d express the orientation of $\boldsymbol{S}^*$ and $\boldsymbol{D}^*$ vectors in the $\{S_2^*, S_3^*\}$ subspace. $\boldsymbol{D}^*$ is normal to the equipotential surface ϕ = constant.

For two different samples ($\delta_s = 0°$ and $\delta_s = 10°$), we now prescribe a stress state of the form $\boldsymbol{S}^* = (0,S_2^*,S_3^*,0,0)$, corresponding to the superposition of a uniaxial compression in the $z'z$ direction and a shear in the $y'y$ direction. We define the angle ψ_s, in a similar way to ψ_d, to express the orientation of the stress vector $\boldsymbol{S}^*$ (Fig. 4). Fig. 5a shows how the angle ψ_d varies with ψ_s, for both samples. For $\delta_s = 0°$, we distinguish two different domains for the mechanical behavior. The first domain corresponds to $15° \leq \psi_s \leq 165°$, i.e. to stress states for which $S_3^* \geq S_2^*/4$. We find that $83° \leq \psi_d \leq 96°$, indicating that $D_3^* \geq 8D_2^*$. Here, the direction of $\boldsymbol{D}^*$ varies only slightly with the direction of $\boldsymbol{S}^*$, and the sample hardly deforms axially. In the second domain, corresponding to $-15° \leq \psi_s \leq 15°$ and $165° \leq \psi_s \leq 195°$ (i.e. mainly axially stressed samples), a very different behavior is found. The direction of the strain rate is highly sensitive to the direction of $\boldsymbol{S}^*$. A variation of the applied stress direction of only 30° leads to a drastic change of $\sim 180°$ in the strain rate direction (i.e. leads to roughly the opposite strain rate vector). Note that such a behavior cannot be obtained by introducing an enhancement factor in the isotropic Glen flow law, since, in that case, the $\boldsymbol{S}^*$ and $\boldsymbol{D}^*$ vectors are necessarily parallel, i.e. ψ_s and ψ_d are equal. For $\delta_s = 10°$, a globally similar behavior is obtained, but one important difference arises: none of the $\{S_1^*,S_2^*\}$ and $\{S_3^*\}$ subspaces are closed. For example, when performing a stress-imposed shear test (i.e. for $\psi_s = 90°$), $\psi_d = 73°$, indicating a significant axial deformation (extension) in the $z'z$ direction. Similarly, when performing a strain-imposed shear test (i.e. for $\psi_d = 90°$), $\psi_s = 156°$, indicating a significant (compressive) axial stress S_2^*. According to Fig. 5b, these two shear tests lead to significantly different flow stresses. We find $S_3^*/\sigma_0 = 0.55$ for $\psi_s = 90°$, but $S_3^*/\sigma_0 = 0.86$ for $\psi_d = 90°$. The enhancement factor deduced from testing under the latter conditions (which correspond to the experiments of Lile [29] and Russel-Head and Budd [30]) is ~ 6 times lower than that deduced from the first test conditions. This feature is not observed for $\delta_s = 0°$ owing to the closedness of $\{S_3^*\}$. We can also show that torsion tests, as performed up to now in Grenoble, are not ideal tests for strongly textured samples. Indeed, in the case of torsion, the prescribed shear stress does not have a constant orientation with respect to the sample axes. Since the torsion axis is generally not a revolution axis for the

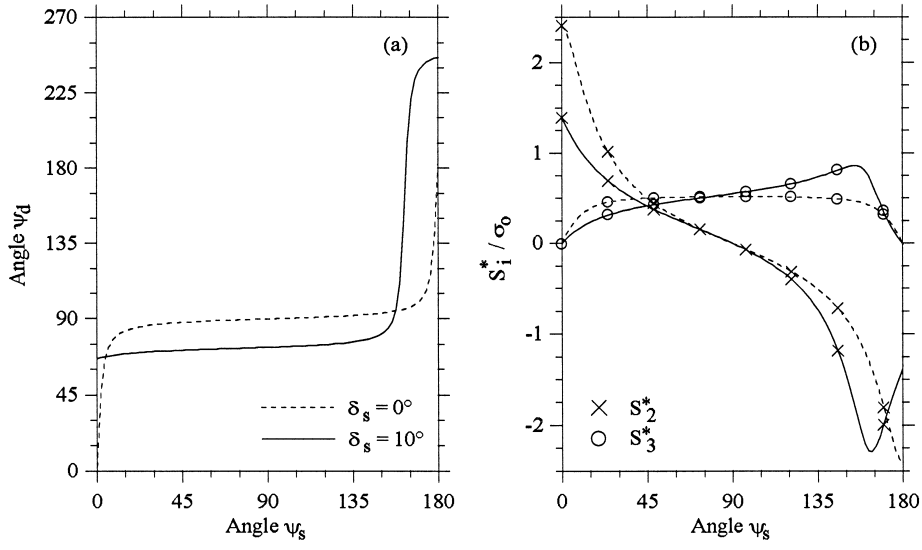

Fig. 5. Response of polycrystals exhibiting axisymmetric textures of similar concentration, calculated with the VPSC model for $\delta_s = 0°$ and $\delta_s = 10°$.
(a) Direction of the $\boldsymbol{D}^*$ vector in the $\{S_2^*,S_3^*\}$ subspace.
(b) Evolution of S_2^*/σ_0 and S_3^*/σ_0 components with the angle ψ_s.

texture, a heterogeneously distributed axial strain (and/or stress) should appear within the sample.

To sum up this subsection, it is found that: (1) no subspace can be assumed to be closed for natural ice samples exhibiting an approximately axisymmetric texture (samples sometimes deform in a direction that is very different from the direction of the prescribed stress); and (2) the behavior of strongly textured polycrystals is extremely sensitive (respectively poorly sensitive) to the orientation of the texture with respect to the prescribed stress when the sample is in ''hard glide'' (resp. ''easy glide'') orientation. These features can induce significant inaccuracies on results of mechanical tests if special care is not taken. In the next section, we qualitatively estimate the influence of ice anisotropy on the large-scale flow in the vicinity of the GRIP drill site. Since ice textures are assumed to be axisymmetric around the in situ vertical axis, results presented below are to be taken only as a first approximation of what anisotropy can do.

4. Influence on in situ flow

We will now use the large-scale ice flow model of Mangeney et al. [13,14] to calculate the flow of ice in the vicinity of the GRIP drill site. This 2-dimensional model does not use the shallow ice approximation generally adopted in glaciology, which is based on the existence of a small aspect ratio in ice sheet geometry. The model presents the particularity of completely solving the set of stress equilibrium and incompressibility equations, which renders it applicable to any ice sheet and bedrock topography. Furthermore, it takes into account an anisotropic constitutive relation, developed by Lliboutry [15], which describes the macroscopic behavior of the ice for a given texture, but not the texture development with the deformation history. This constitutive relation is applicable to ices with axisymmetric textures. It is based on a homogenization method, assuming a uniform stress within the polycrystal, and is used here in the case of Newtonian viscosity ($n = 1$). It is worth pointing out that uniform stress models do not take into account intergranular interaction effects, as the VPSC model does. According to Mangeney [31], Lliboutry's constitutive relation underestimates the anisotropy of polar ices, since the enhancement factor of strongly textured samples varies by less than one order of magnitude with the direction of the prescribed stress, instead of more than two orders of magnitude as observed experimentally. The large-scale flow model was applied along the GRIP–GISP2 flow line, for a prescribed temperature field, bedrock topography, and accumulation rate (those measured in situ), under steady-state conditions, and with no sliding at the ice sheet/bedrock interface. Textures are assumed to be axisymmetric around the in situ $z'z$ vertical axis, and the texture concentration input in the model was fitted to reproduce the steady texture development measured at GRIP. It is worth emphasizing that: (1) the texture patterns are not updated with the calculated velocity field; (2) the 250 m thick layer of warm recrystallized ice, which exhibits a less anisotropic behavior, is not taken into account; and (3) the temperature field is not calculated. Due to these simplifications and to the particular texture symmetry we assume, results cannot presently be used for comparison with observations. However, comparison of the flows calculated with isotropic and anisotropic constitutive relations leads to interesting remarks.

The calculated shear strain rates D_{xz} ($x'x$ is the horizontal axis) are plotted in Fig. 6 for both isotropic and anisotropic cases. We see that in the vicinity of the GRIP drill site, the isoline $D_{xz} = 0$ has a more sinuous shape in the anisotropic case, and that D_{xz} is generally not zero along the GRIP bore hole. Near the bedrock, for $-10\ \text{km} \le x \le 10\ \text{km}$, isolines obtained in both isotropic and anisotropic cases are far from being superimposed. Farther from the GRIP drill site, the isolines are flatter in the anisotropic case. Note that these features should be more marked with a constitutive relation that does not underestimate ice anisotropy.

Let us now use the conclusions of previous sections to explain these results. Anisotropic flow is calculated here for conditions $\delta_s = 0°$ which corresponds, as shown above, to an idealized case. The ice only deforms axially along the $D_{xz} = 0$ isoline. On the other hand, ice is strongly anisotropic in the last 1000 m of the ice sheet. Along the $D_{xz} = 0$ isoline, the deep ice is thus stressed in conditions for which the strain rate direction is highly sensitive to the stress direction, as shown in Section 3.3. Further-

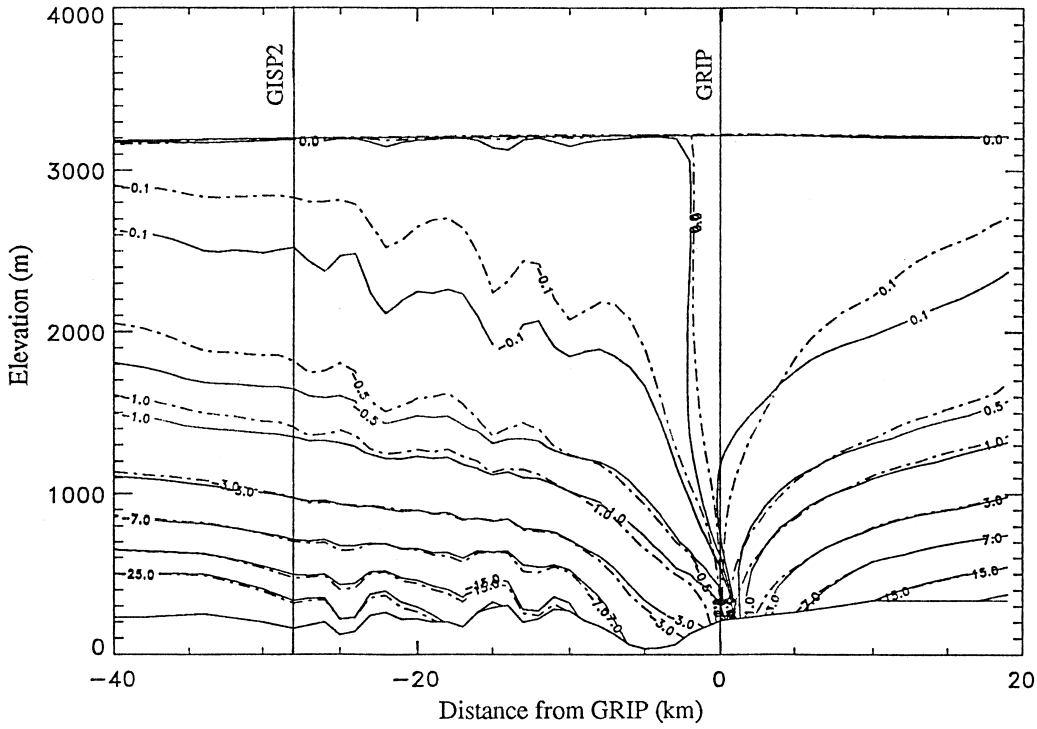

Fig. 6. Isovalues of the shear strain rate D_{xz} (in 10^{-4} yr^{-1}) in a vertical section of the GRIP–GISP2 flowline, calculated with both an isotropic (– · –) and an anisotropic (–––) constitutive relation.

more, the irregular bedrock topography locally influences the stress field, particularly in deep layers. Therefore, in deep ice layers of the ice divide region, the direction of the strain rate is highly sensitive to the bedrock topography, and a large shear strain rate may appear even exactly below the summit of the ice sheet where the shear stress is expected to be small. In a similar way, the strain rate direction is expected to be highly sensitive to the orientation of the texture (which may also be influenced by the bedrock topography since the bedrock locally modifies the deformation path of the ice) with respect to the in situ vertical axis. The flow of deep ices in the ice divide region is thus characterized by a high sensitivity which probably makes it quite complex. For example, a slight migration of the ice sheet summit due to some climatic changes, as studied by Anandakrishnan et al. [32], could lead to a drastic change in the flow pattern. This complexity of the flow should increase the difficulty of interpreting climatic data measured along GRIP-like cores. In particular, it could enhance mixing in deep ice layers, i.e. disturbing the stratigraphy.

Farther from the ice divide, the horizontal shear stress is dominant in deep layers. The strain rate direction is thus only slightly sensitive to stress direction, as shown in Section 3.3. Consequently, bedrock topography should have little influence on strain rate direction, i.e. on the flow pattern. Similarly, texture orientation has much less influence on flow than in the ice divide region. This feature is likely to explain (at least partly) why the stratigraphy of deep layers is not disturbed over more than 50 m above bedrock at Dye 3, where ice flows essentially by shear over an irregular bedrock with 500 m high relief [33], and why the stratigraphy is disturbed 300 m over bedrock at GRIP and GISP2 [34], where ice was initially thought to flow mainly vertically downwards, i.e. where the flow was thought to be less influenced by the bedrock.

Therefore, the flow of ice in the ice divide region cannot be accurately modelled without a constitutive

relation that *precisely* describes texture development with deformation history. In particular, this constitutive relation should take into account the influence of all dynamic recrystallization regimes on texture development [9]. At present, such a relation is not available.

5. Conclusions

We have presented results of several experimental tests performed in two different laboratories (LGGE-Grenoble and Kitami Institute of Technology) on GRIP ice samples. These tests make it possible to estimate the directional viscosities corresponding to a nearly vertical in situ compression and to an in situ horizontal shear combined with a horizontal uniaxial tension. We observe a gradually increasing anisotropy from 1000 down to 2600 m depth, and a slightly decreasing anisotropy below. A qualitative correlation between rheology and texture concentration has been found. In horizontal shear, GRIP ices are surprisingly soft, probably due to the differential flow in cloudy band layer ice. We have used the ViscoPlastic Self-Consistent (VPSC) model to describe the instantaneous behavior of textured samples in a more general way. This model makes it possible to estimate all components of the strain rate tensor under experimental conditions, and to examine the sensitivity of the mechanical response to specific texture parameters. The model well reproduces the qualitative dependence of the rheology of GRIP samples on the texture, whereas an excellent quantitative agreement was found with the tests performed under Grenoble-like test conditions. We have shown that under these conditions, samples mainly deform by shear in response to a compressive stress. This shear deformation is due to a slight misorientation of the texture axis with respect to the compression axis. Under Kitami-like tests conditions and for strongly textured samples, the ice mainly deforms axially. The latter test conditions therefore give lower experimental inaccuracy, as compared for example to torsion tests, when estimating the directional viscosity corresponding to an in situ horizontal shear. Finally, we applied a large-scale flow model to Central Greenland to understand how anisotropy may really influence the flow in ice sheets. Owing to the particular behavior of anisotropic ices and to the prescribed stress regime, the flow of ice in the ice divide region is expected to be extremely sensitive to bedrock topography, texture orientation, and position of the ice sheet summit. Such a feature is not found far from the ice divide. The complexity of the flow near the ice divide could largely help the formation of stratigraphic disturbances. One should then expect that climatic data measured in the deepest part of ice cores drilled near an ice divide region cannot be dated or interpreted with present large-scale flow models. Consequently, ice divide regions are probably not the most appropriate drill sites. The understanding of the influence of ice anisotropy on flow in ice sheets is essentially limited at present by the lack of a complete anisotropic constitutive relation that describes texture development in a general way, in other words for all deformation and recrystallization regimes observed in ice sheets.

Acknowledgements

This work is a contribution to the GReenland Ice-core Project, carried out at Summit, central Greenland. Financial support was provided by the national funding bodies of Belgium, Denmark, France, Germany, Iceland, Italy, Switzerland, and the United Kingdom, under the auspices of the European Science Foundation. This work was also supported by the PNEDC (Programme National d'Étude de la Dynamique du Climat) CNRS, and by the CEC (Commission of European Communities) Environment Program. We are very grateful to G.R. Canova and R.A. Lebensohn for allowing us to use their VPSC code and for very fruitful discussions. ***[AC]***

Appendix A. Deformation of $\delta_s = 45°$ samples

We consider a sample exhibiting an axisymmetric texture corresponding to $\delta_s = 45°$, and we deform it under uniaxial compression in the $z'z$ direction. These conditions correspond to idealized Kitami experiments. We define the reference frame $(Ox^1y^1z^1)$ such that $(Ox^1) = (Ox)$ and that (Oz^1) is the revolution axis of the texture (Fig. 7). According to Canova et al. [28], $\{S_1^*, S_2^*, S_3^*\}$, $\{S_1^{*1}, S_2^{*1}\}$, $\{S_3^{*1}\}$, and

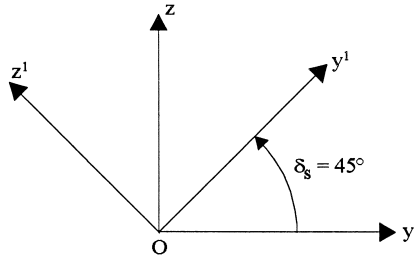

Fig. 7. The (Oz) axis corresponds to the compression axis, and (Oz^1) to the revolution axis of the texture.

$\{S_1^{*1},S_2^{*1},S_3^{*1}\}$ subspaces are closed. The applied deviatoric stress along the $(Oxyz)$ axes:

$$\boldsymbol{S}=\begin{bmatrix} -S_{33}/2 & 0 & 0 \\ 0 & -S_{33}/2 & 0 \\ 0 & 0 & S_{33} \end{bmatrix} \tag{18}$$

reads in the $(Ox^1y^1z^1)$ axes:

$$\boldsymbol{S}^1=\frac{1}{4}\begin{bmatrix} -2S_{33}/2 & 0 & 0 \\ 0 & S_{33} & -3S_{33} \\ 0 & -3S_{33} & S_{33} \end{bmatrix} \tag{19}$$

i.e. has the form $\boldsymbol{S}^1=(S_1^1;S_2^1;S_3^1;0;0)$. Thus, $\boldsymbol{S}^1$ corresponds to superimposing a shear stress S_{23}^1 with a uniaxial tensile stress in the (Ox^1) direction. Since $\{S_1^{*1},S_2^{*1},S_3^{*1}\}$ is a closed subspace, $\boldsymbol{D}^1$ takes the following form in $(Ox^1y^1z^1)$:

$$\boldsymbol{D}^1=\begin{bmatrix} D_{11}^1 & 0 & 0 \\ 0 & D_{22}^1 & D_{23}^1 \\ 0 & D_{23}^1 & D_{33}^1 \end{bmatrix} \tag{20}$$

with $D_{11}^1+D_{22}^1+D_{33}^1=0$, and therefore reads as follows in $(Oxyz)$:

$$\boldsymbol{D}=\frac{1}{2}\begin{bmatrix} 2D_{11}^1 & 0 & 0 \\ 0 & 2D_{23}^1-D_{11}^1 & D_{33}^1-D_{22}^1 \\ 0 & D_{33}^1-D_{22}^1 & -2D_{23}^1-D_{11}^1 \end{bmatrix} \tag{21}$$

If the texture of the polycrystal is sufficiently concentrated, then the sample hardly deforms axially in the $(Ox^1y^1z^1)$ axes as compared to the case of shear parallel to the y^1z^1 plane. Since all non-zero components of $\boldsymbol{S}^1$ are of the same order, D_{ii}^1 components are at least one order of magnitude lower than D_{23}^1, leading to negligible values of $D_{23}=D_{33}^1-D_{22}^1$ as compared to $D_{22}=2D_{23}^1-D_{11}^1$ or $D_{33}=-2D_{23}^1-D_{11}^1$. Therefore, a $\delta_s=45°$ sample mainly deforms axially in response to a compressive stress if its texture is sufficiently concentrated.

References

[1] P. Pimienta, P. Duval, V.Y. Lipenkov, Mechanical behavior of anisotropic polar ice, in: The Physical Basis of Ice Sheet Modelling, Int. Assoc. Hydrol. Sci., Vancouver, BC, 1987, Publ. 170, pp. 57–66.

[2] H. Shoji, C.C. Langway, Mechanical properties of fresh ice core from Dye 3, Greenland, in: C.C. Langway, Jr., H. Oeschger, W. Dansgaard (Eds.), Geophysical Monograph, Geophysics, Geochemistry, and the Environment, vol. 33, Am. Geophys. Union, Washington, DC, 1985, pp. 39–48.

[3] W.F. Budd, T.H. Jacka, A review of ice rheology for ice sheet modelling, Cold Reg. Sci. Technol. 16 (1989) 107–144.

[4] P. Duval, O. Castelnau, Dynamic recrystallization of ice in polar ice sheets, J. Phys. (Paris) IV C3 (5) (1995) 197–205.

[5] R.B. Alley, A.J. Gow, D.A. Meese, Mapping *c*-axis fabrics to study physical processes in ice, J. Glaciol. 41 (112) (1995) 425–433.

[6] R.B. Alley, A.J. Gow, S.J. Johnsen, J. Kipfstuhl, D.A. Meese, Th. Thorsteinsson, Comparison of deep ice cores, Nature (London) 373 (1995) 393–394.

[7] D. Dahl-Jensen, Th. Thorsteinsson, R. Alley, H. Shoji, Flow properties of the ice from the GRIP ice core — the reason for folds? J. Geophys. Res. (in press, 1996).

[8] R.A. Lebensohn, C.N. Tomé, A self-consistent anisotropic approach for the simulation of plastic deformation and texture development of polycrystals: application to zirconium alloys, Acta Metall. 41 (9) (1993) 2611–2624.

[9] O. Castelnau, P. Duval, R.A. Lebensohn, G.R. Canova, Viscoplastic modelling of texture development in polycrystalline ice with a self-consistent approach; comparison with bound estimates, J. Geophys. Res. 101 (B6) (1996) 13851–13868.

[10] O. Castelnau, Th. Thorsteinsson, J. Kipfstuhl, P. Duval, G.R. Canova, Modelling texture development along the GRIP ice core (central Greenland), Ann. Glaciol. 23 (1996) 194–201.

[11] O. Castelnau, G.R. Canova, R.-A. Lebensohn, P. Duval, Modelling viscoplastic behavior of anisotropic polycrystalline ice with a self-consistent approach, Acta Mater. 45 (11) (1997) 4828.

[12] N. Azuma, K. Goto-Azuma, An anisotropic flow law for ice-sheet ice and its implications, Ann. Glaciol. 23 (1996) 202–208.

[13] A. Mangeney, F. Califano, O. Castelnau, Isothermal flow of an anisotropic ice sheet in the vicinity of an ice divide, J. Geophys. Res. 101 (B12) (1996) 28189–28204.

[14] A. Mangeney, F. Califano, K. Hutter, A numerical study of anisotropic, low Reynolds number, free surface flows for ice sheet modelling, J. Geophys. Res. (submitted, 1996).
[15] L. Lliboutry, Anisotropic, transversely isotropic nonlinear viscosity of rock ice and rheological parameters inferred from homogenization, Int. J. Plasticity 9 (1993) 619–632.
[16] S. Anandakrishnan, J.J. Fitzpatrick, R.B. Alley, A.J. Gow, D.A. Meese, Shear-wave detection of asymmetric *c*-axis fabrics in the GISP2 ice core, Greenland, J. Glaciol. 40 (136) (1994) 491–496.
[17] Th. Thorsteinsson, J. Kipfstuhl, H. Miller, Textures and fabrics in the GRIP ice core, J. Geophys. Res. (in press, 1996).
[18] P. Duval, M.F. Ashby, I. Anderman, Rate-controlling processes in the creep of polycrystalline ice, J. Phys. Chem. 87 (21) (1983) 4066–4074.
[19] Ph. Lequeu, P. Gilormini, F. Montheillet, B. Bacroix, J.J. Jonas, Yield surfaces for textured polycrystals, I. Crystallographic approach, Acta Metall. 35 (2) (1987) 439–451.
[20] D. Dahl-Jensen, Two dimensional thermo-mechanical modelling of flow and depth–age profiles near the ice divide in central Greenland, Ann. Glaciol. 12 (1989) 31–36.
[21] H. Legac, Contribution à la détermination des lois de comportement de la glace polycristalline (anélasticité et plasticité), Ph.D. Thesis, Université Scientifique et Médicale de Grenoble, Grenoble, 1980.
[22] L. Lliboutry, P. Duval, Various isotropic and anisotropic ices found in glaciers and polar ice caps and their corresponding rheologies, Ann. Géophys. 3 (2) (1985) 207–224.
[23] H. Shoji, C.C. Langway, Flow law parameters of the Dye 3. Greenland, deep ice core, Ann. Glaciol. 10 (1988) 146–150.
[24] H. Shoji, C.C. Langway, Flow velocity profiles and accumulation rates from mechanical tests on ice core samples, in: The Physical Basis of Ice Sheet Modelling, Int. Assoc. Hydrol. Sci., Vancouver, BC, 1987, Publ. 170, pp. 67–77.
[25] A. Molinari, G.R. Canova, S. Ahzi, A self-consistent approach of the large deformation polycrystal viscoplasticity, Acta Metall. 35 (12) (1987) 2983–2994.
[26] J.D. Eshelby, The determination of the elastic field of an ellipsoidal inclusion, and related problems, Proc. R. Soc. London, Ser. A 241 (1957) 376–396.
[27] O. Castelnau, Modélisation du comportement mécanique de la glace polycristalline par une approche auto-cohérente; application au développement de textures dans les glaces des calottes polaires, Ph.D. Thesis, Université Joseph Fourier (Grenoble 1), Grenoble, 1996.
[28] G.R. Canova, U.F. Kocks, C.N. Tomé, J.J. Jonas, The yield surface of textured polycrystals, J. Mech. Phys. Solids 33 (4) (1985) 371–397.
[29] R.C. Lile, The effect of anisotropy on the creep of polycrystalline ice, J. Glaciol. 21 (85) (1979) 475–483.
[30] D.S. Russell-Head, W.F. Budd, Ice-flow properties derived from bore-hole shear measurement combined with ice-core studies, J. Glaciol. 24 (90) (1979) 117–130.
[31] A. Mangeney, Modélisation de l'écoulement de la glace dans les calottes polaires: prise en compte d'une loi de comportement anisotrope, Ph.D. Thesis, Université Pierre et Marie Curie (Paris VI), Paris, 1996.
[32] S. Anandakrishnan, R.B. Alley, E.D. Waddington, Sensitivity of the ice-divide position in greenland to climate change, Geophys. Res. Lett. 21 (6) (1994) 441–444.
[33] W. Dansgaard, H.B. Clausen, N. Gundestrup, S.J. Johnsen, C. Rygner, Dating and climatic interpretation of two Greenland ice cores, in: C.C. Langway, Jr., H. Oeschger, W. Dansgaard (Eds.), Greenland Ice Core, Geophysics, Geochemistry, and the Environment, Am. Geophys. Union, Washington, DC, Washington DC, 1985, Geophys. Monogr. 33, pp. 71–76.
[34] P.M. Grootes, M. Stuiver, J.W.C. White, S.J. Johnsen, J. Jouzel, Comparison of oxygen isotope records from the GISP2 and GRIP Greenland ice cores, Nature (London) 366 (1993) 552–554.